Control Engineering Practice 174 (2026) 107052

Contents lists available at ScienceDirect

Control Engineering Practice

journal homepage: www.elsevier.com/locate/conengprac

Model predictive control of anaerobic co-digestion: Experimental validation of a robust tube-based scheme

D. Carecci [a,*], L. Dewasme [b], E. Ficara [c], A. Vande Wouwer [b], G. Ferretti [a], S. García-Gen [d]

[a] Department of Electronics, Information and Bioengineering (DEIB), Politecnico di Milano, Piazza Leonardo da Vinci 32, Milan, Italy
[b] Systems, Estimation, Control and Optimization (SECO), University of Mons (UMONS), Boulevard Dolez 31, 7000, Mons, Belgium
[c] Department of Civil and Environmental Engineering (DICA), Politecnico di Milano, Piazza Leonardo da Vinci 32, Milan, Italy
[d] Departamento de Ingeniería Química y Ambiental, Universidad Técnica Federico Santa María, Avenida España 1680, Valparaíso, Chile

ARTICLE INFO

Keywords:
Biomethane
Anaerobic co-digestion
Robust control
Experimental validation
NMPC
EKF

ABSTRACT

Modeling, optimization and control tools may play a key role in improving the techno-economic performance of biomethane production via the anaerobic co-digestion process, helping to deal with the challenges that such plants will face in the next decades. Due to the intrinsic complexity of the process and associated safety considerations, industrial practice typically adopts conservative loading conditions that remain well below the maximum production potential. The objective is to safely modify the input diet to track improvements in biomethane flow rate. As model-based and predictive control techniques are of interest due to their inherent ability to optimize a cost function while ensuring constraint satisfaction, this study presents the experimental validation of a tube-based nonlinear model predictive controller (NMPC) for the anaerobic co-digestion of agro-industrial feedstocks. The NMPC framework employs a predictor based on a simple two-stage anaerobic digestion model extended with the hydrolytic step of multiple co-feedstocks, whereas the setpoints are set by an *offline* optimization carried out with a high-fidelity model. The controller is combined with an Extended Kalman Filter (EKF) which uses only biogas flow and composition data to estimate the unmeasurable states. A successful application of the proposed control scheme to a real bench-scale reactor is presented and benchmarked against a previously validated PI-based strategy.

1. Introduction

According to the Statistical Report by the European Biogas Association (EBA), renewable biogas and biomethane could cover 35–62% of gas demand in Europe by 2050, thereby shaping the next energy mix to support the transition to an integrated net-zero energy system (European Biogas Association, 2024). Anaerobic digestion (AD) is a mature process in which a microbial consortium converts the biodegradable components of organic wastes and biomass by-products into biomethane and biogenic carbon dioxide (biogas), and bio-fertilizer (digestate): this helps to reduce the carbon footprint of the agricultural and waste sectors, as the methane naturally emitted from organic wastes is captured in a controlled environment instead of being released into the atmosphere (Abbasi et al., 2012). AD of complex feedstocks entails a convoluted cascade of slow (in the order of hours–days) and complex biochemical reactions.

Given the metabolic needs of the microbial consortium, the input diet for the reactors shall be well balanced in terms of elemental composition (carbon (C), nitrogen (N), phosphorus (P), and inorganics/trace metals). It follows that the anaerobic co-digestion (AcoD) of multiple feedstocks techno-economically out-competes mono-digestion and is now well established in industrial practice (Vavilin & Lokshina, 1996). However, from the perspective of the reduction/loss of incentive schemes after 2030, a fixed co-digestion diet may no longer be economically viable. Indeed, in the next decades, the challenge to improve the techno-economic performance of biomethane plants requires a dynamic adaptation of the input diet, under the identification of the optimal trade-off between high-yield (ultimate Biochemical Methane Potential BMP_∞ in $Nm^3_{CH_4}$ ton^{-1}) and low cost (purchase/transportation in €ton^{-1}) feedstock mixtures, i.e., being able to improve the biomethane production with minimum operational cost. This holds in particular for reactors fed with agro-industrial feedstocks (e.g., animal slurries, energy crops, industrial

* Corresponding author.
E-mail addresses: davide.carecci@polimi.it (D. Carecci), laurent.dewasme@umons.ac.be (L. Dewasme), elena.ficara@polimi.it (E. Ficara), alain.vandewouwer@umons.ac.be (A. Vande Wouwer), gianni.ferretti@polimi.it (G. Ferretti), santiago.garciage@usm.cl (S. García-Gen).

https://doi.org/10.1016/j.conengprac.2026.107052
Received 3 January 2026; Received in revised form 30 March 2026; Accepted 6 May 2026
Available online 15 May 2026

by-products), which are the focus of this work since they represent the largest portion of the EU's installed capacity (European Biogas Association, 2024).

Dynamic co-digestion, as mono-digestion, requires strict control of operating conditions using multiple regulations involving variables such as temperature, pH, nutrient availability, organic loading rate (OLR), and dilution rate (D) (Ibarra-Esparza et al., 2025). AcoD control is challenging due to the presence of non-linear, non-monotonic static relationships between biomethane production and OLR. Insufficient or excessive OLR may limit methane production due to the corresponding limitation or over-accumulation of volatile fatty acids (VFAs). The latter is a critical intermediate product of the bioreaction chain, and its concentration is usually considered as the main process health indicator (Ahring et al., 1995; Alavi-Borazjani et al., 2020; Kazemi et al., 2020; Weinrich & Nelles, 2021). To maintain VFA concentration within an acceptable range, conservative and suboptimal loading conditions may be considered, well below the maximum production potential. Optimal operation control of such facilities presents a dual objective: maximizing biomethane production and maintaining stable/safe conditions. In addition, the incentive granting is constrained by environmental sustainability on both the influent diet mixture and the effluent digestate compositions (e.g., Total Ammonia Nitrogen (TAN), Chemical Oxygen Demand (COD)). In this framework, model predictive control (MPC) seems to be the most suitable algorithm for tackling the control problem, owing to its ability to minimize a cost function while explicitly enforcing input, state, and output constraints.

However, due to the process's limited economic performance and the still-high cost of many sensors in biochemistry, poor instrumentation, control, and automation (ICA) are usually present in full-scale plants. Only a few data are collected at high-frequency, i.e. *online* (e.g., biogas flow rate and composition), while the majority of the monitoring quantities are still measured manually at low-frequency, i.e., *offline*, such as inhibitors' concentrations (VFAs, TAN), other proxies of the reactors' state-of-health (pH, intermediate (IA) over total (TAC) alkalinity ratio or *FOS/TAC*) and digestate quality (total (TS) and volatile (VS) solids, TAN, COD). In addition, since steady-state operations are normally maintained, the data are usually poorly informative regarding the complexity of the process. This poses challenges in identifying observable, reliable models and, in turn, in applying advanced/data-driven control techniques, thereby limiting their spread in favor of more conventional, local control schemes.

Coherently with such lack of data, literature has primarily focused on developing comprehensive first-principle models rather than data-driven ones: among others, the *IWA Anaerobic Digestion Model No. 1* (ADM1) (Batstone et al., 2002) model remains the state-of-the-art of AD modeling, with a detailed description of all 4 main cascade reaction stages: hydrolysis → acidogenesis → acetogenesis → methanogenesis. Since its original formulation, the literature has been enriched with model extensions (e.g., Bułkowska et al., 2018; Carecci et al., 2024b) and applications to many different feedstocks and operating conditions (Kegl et al., 2025). As a result, the goodness of its open-loop predictive ability was extensively assessed, as well as its lack of full observability and poor practical identifiability (Nimmegeers et al., 2017). As it is common for bioprocess modeling, the lack of informative data results in large parameter uncertainties (Dochain & Vanrolleghem, 2005), especially on kinetics (Barahmand & Samarakoon, 2023).

The literature is rich in studies proposing different control algorithms for the AD process (Jimenez et al., 2015), but no single state-of-the-art approach has been established yet. Moreover, in general, many works focus on the mono-AD of easily biodegradable soluble wastes, and/or consider hypotheses that prevent their direct applicability in full-scale agro-industrial AcoD plants (e.g., *online* measurability of total VFA (TVFA) and biodegradable soluble COD, and/or control actions such as alkali supplementation Ahmed & Rodríguez, 2020; Zhou et al., 2020). From a review of the Scopus database, clear literature gaps emerged on MPC applications to AcoD and related experimental validations. Indeed, the vast majority of works either (i) rely on simulation studies with the ADM1 model (which holds essentially in steady-state operations, whereas it has stronger limitations in predicting transient dynamic responses Arzate et al., 2017; Carecci et al., 2025b), or (ii) consider process models that are inadequate to describe the system treating complex feedstocks and facing time-varying AcoD operations. They typically focus on the AD of simple/easily biodegradable wastes, neglecting the presence of intermediate inhibitors (Mauky et al., 2016) or rate-limiting stages such as hydrolysis (e.g., the AM2 model Bernard et al., 2001). Further details are reported in Table S1 of the Supplementary Material (SM).

As the majority of the digestate characteristics, i.e., states in first principle models such as substrates and microbial biomasses, are often not measurable *online*, state observers (Bogaerts & Wouwer, 2003) are required to provide the full state information to the MPC loop. This reduces the choice of process models for real-time operations to those that highlight good observability properties and sufficient predictive ability, balancing complexity and tractability (Dochain & Vanrolleghem, 2005). The two-step reaction core of the original AM2 model was shown to be observable based on the sole measurement of the biomethane flow rate (q_M) (Dewasme et al., 2019). The latter has therefore been frequently proposed for control-oriented purposes. However, an increase in the model's dimensionality was deemed necessary to improve predictive capability under time-varying AcoD operations, leading the authors to consider the more complex AM2HN model (Hassam et al., 2015). Many AM2-based state observers have been proposed for the AD process (e.g., standard Bayesian, asymptotic, interval, sliding mode) (Jimenez et al., 2015), but their direct applicability to the considered case studies is often hindered because they usually rely on unverified assumptions. More details are reported in Section I of the SM.

Model uncertainties, coupled with nonlinear dynamics, degrade the performance of MPC strategies, leading to constraint violations (or problem infeasibility) and, in turn, suboptimal or unsafe operation. A robust formulation is therefore advised, among which the *tube paradigm* stands out as a computationally efficient approach under boundedness assumption on model disturbances, maintaining recursive feasibility and constraint compliance (Dewasme et al., 2024; Mayne et al., 2011). Only a few contributions of robust MPC to the AD process have been reported in the literature, such as multi-scenario (Hellmann et al., 2026; Piceno-Díaz et al., 2020) and tube-based (Carecci et al., 2025a) approaches, which address uncertainties in kinetic parameters or influent composition.

In this work, following structural observability analysis, a structurally observable reduced-order–yet sufficiently comprehensive–nonlinear state-space model for the AcoD of agro-industrial feedstocks is derived. The first contribution of the present work is the design and validation of a full-order state observer based on this model. The second, more important contribution is the experimental validation, using a bench-scale reactor, of the robust tube-based NMPC initially designed in a previous work (Carecci et al., 2025a). The limited additional implementation requirements and the dual objective of improving biomethane production while ensuring process stability under dynamic feeding conditions make the proposed approach appealing for practical full-scale deployment. The experimental results of the NMPC are benchmarked using a parallel reactor run under the same operating conditions and controlled by the single-input single-output (SISO) *selector-PI* approach described and validated in Carecci et al. (Carecci et al., 2024a).

Section 2 briefly reviews the modeling framework and the materials and methods used in the experimental work. Section 3 then details the development of the predictor, state observer, and NMPC policies subsequently employed for real-time control. Preliminary results and the numerical validation of the state observer and its closed-loop integration with the NMPC are presented in Section 4, followed by the actual experimental results discussed in Section 5. Eventually, the main conclusions and prospects are reported in Section 6. To improve readability,

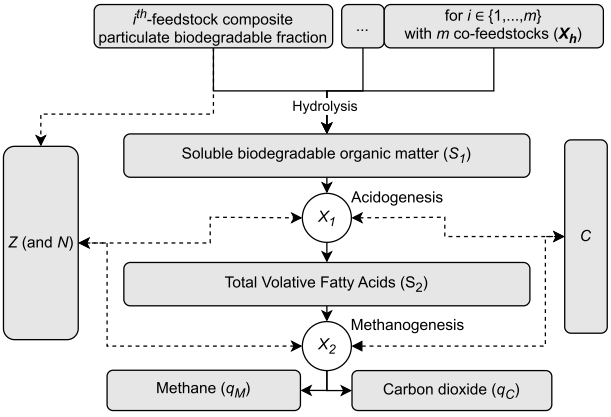

Fig. 1. Simplified representation of the AcoD process based on the AM2HN$_{tan}$ state variables.

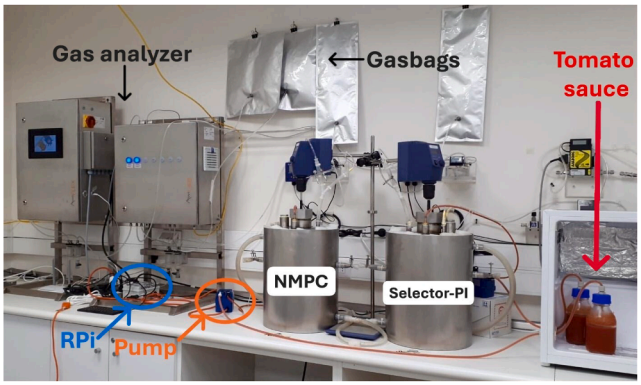

Fig. 2. Picture of the bench-scale reactor during the experimental campaign.

extensive methodological details and additional results are provided in the SM.

2. Materials and methods

2.1. Modeling framework

Two gray-box first-principles models were considered: (i) a high-fidelity model used for *offline* optimization and numerical validation, characterized by poor observability and identifiability properties; and (ii) a reduced-order control-oriented model providing a trade-off between predictive capability and structural observability for state estimation and model-based control.

The agri-AcoDM (Carecci et al., 2024b, 2025b), derived from ADM1, serves as the high-fidelity reference: a 43-state nonlinear DAE system in a CSTR that describes comprehensively the 4 main stages of the process cascade, with algebraic equations for acid-base equilibrium and charge neutrality, and nonlinearities arising from pH computation, precipitation kinetics and Monod/Haldane microbial kinetics.

For control design, the reduced-order AM2HN and AM2HN$_{tan}$ models (Carecci et al., 2025b; Hassam et al., 2015) were primarily considered. They capture the main process dynamics (hydrolysis → acidogenesis → methanogenesis) while preserving the main input-output structure of the high-fidelity model, at the cost of lumping, for example, 7 microbial populations into 2 and 4 individual VFAs into one (Bornhöft et al., 2013). Haldane kinetics describe the methanogenesis step, discriminating between limited and inhibited operating regions with respect to the TVFA (acetate-equivalent) concentration. In the AM2HN$_{tan}$ version, an additional state that describes the dynamics of TAN is present to include free ammonia (NH_3) inhibition in the methanogens' growth rate (μ_2) expression (modeled as a multiplicative non-competitive function).

Model uncertainty may arise from both influent characterization ($\boldsymbol{\theta_{in,i}}$, for each co-feedstock $i \in \{1,\dots,m\}$) and stoichiometric/kinetic process parameters ($\boldsymbol{\theta_P}$). As good characterization of each co-feedstock is usually available in industrial practice (even though with infrequent updates, e.g., seasonal), kinetics was considered the dominant source (Weinrich & Nelles, 2021).

A schematic of the process cascade with reference to the AM2HN$_{tan}$ state variables is shown in Fig. 1; the full description of all models' quantities is provided in Section II.A of the SM.

2.2. Bench-scale plant

The bench-scale plant, shown in Fig. 2, consists of two identical reactors (*digesters*), allowing for parallel continuous experiments. Each digester includes a CSTR and a gas line. Each CSTR is a 15-L metal container with a working volume V of 10–13 L and is equipped with a free-access funnel for manual feeding and a stopper for gas-proof sealing. A manual drain and valve allow digestate discharge. The reactor is stirred by a mechanical mixer with a vertical shaft and rotational speed controller (OS20-Pro, Scilogex). The reactors are heated by hot water circulating in an external thermal chamber, allowing temperature control within mesophilic or thermophilic ranges. The biogas is conveyed via a dedicated gas-line to a gas counter (Milligas Counter MGC-1, Ritter Apparatebau GmbH, Germany). The produced biogas is then collected in a 10-L gasbag from which it is automatically discharged upon reaching 4.5 L of accumulated volume by a gas pump (micro diaphragm gas pump, KNF) which sends it to a gas analyzer (AWIFlex Cool+, Awite Bioenergie GmbH, Germany), returning its composition in terms of %CH_4, %CO_2 (by infrared spectroscopy) and %O_2, H_2 (ppm), H_2S (ppm) (by electrochemical techniques). An auxiliary system (AwiLAB Gas Analysis, Awite Bioenergie GmbH, Germany) enables control of data acquisition from the gas analyzer and the counters of the different parallel reactors.

2.3. Case study

The initial (baseline) operating conditions ($T = 42$ °C, $D = 3.15 \times 10^{-2}$ d^{-1}, OLR $= 2.89$ g_{COD} d^{-1} L^{-1}) of the bench-scale reactors ($V = 12$ L) were designed to replicate those of a real agro-industrial full-scale digester, particularly in terms of OLR and diet composition.

Due to the limited range of controllable actuators available in the laboratory (i.e., peristaltic pumps), the minor OLR fraction normally attributed to TS-rich secondary co-feedstocks was replaced by tomato sauce, as a pseudo-realistic pumpable feedstock at lab scale. The maize silage to cow slurry ratio was nonetheless kept representative of full-scale operations, yielding a diet mix of 45, 26 and 29% on an OLR basis for maize silage, cow slurry and tomato sauce respectively (i.e., $m = 3$ in Sections 2.1 and 3.1).

As a result, tomato sauce was fed via peristaltic pumps as the control action; whereas maize silage and cow slurry were fed manually and impulsively through the reactor head funnel, either daily or three times per week.

The reactors were inoculated (on 16/03/2025) with digestate from the AD of activated sludge, sourced from a nearby wastewater treatment plant. Following an adaptation period with gradual OLR increases, the full initial load was reached after 23 days. Once near-steady-state conditions were established (initial equilibrium), the closed-loop experiment (reactors controlled with the control algorithms and architecture described in Sections 3.3 and 3.4) started on 20/05/2025; the two-week transient ramp of diet change began on 29/05/2025, and the experiment was terminated on 10/07/2025, i.e. after approximately one hydraulic retention time (HRT $= D^{-1} \approx 30$ days) at the final (optimized) equilibrium.

Due to continuity/resolution limitations of the available sensing equipment, gas composition was analyzed every 4.5 L of accumulated biogas (the minimum volume required by the analyzer), while the biogas flow rate was logged every 5 min. In addition to these *online*-available gas measurements ($\tilde{\mathbf{y}}$), *offline* digestate samples (pH, TS, VS, soluble COD, total COD, TAN, VFAs, IA and TAC) were collected manually once or twice per week, prior to manual feeding, for monitoring and validation purposes.

BMP tests (Holliger et al., 2016) were conducted in duplicate to assess the biodegradability of the overall VS content, BMP_∞, and hydrolytic behavior of all co-feedstocks. Further details on feedstock characterization–derived from a consistent integration of experimental measurements and literature-derived values–and the incorporation of its inherent variability (to reflect realistic industrial conditions) are provided in Section II.C of the SM.

2.4. Analytical methods

Routine physicochemical analyses (pH, TS, VS, COD, TAC, and TAN) were performed in accordance with Standard Methods (APHA et al., 2012) and established protocols. VFAs (acetic, propionic, butyric, and valeric acids) were quantified by gas chromatography with flame ionization detection (GC-FID) using a procedure adapted from internal laboratory methods and standard-addition calibration was employed to account for feedstock effects.

BMP tests were conducted under the same T of the bench-scale experimentation using an Automatic Methane Potential Test System (AMPTS II system), enabling continuous and corrected biomethane production measurements for the direct calculation of the BMP_∞. The inoculum-to-feedstock ratio was set to 2.5 (based on VS). Blank bottles containing inoculum only were also included.

Full details on the analytical procedures are reported in Section II.D of the SM.

3. Process digitalization

3.1. An observability-driven model formulation

A model version suitable for state estimation (and in turn output-feedback predictive control) was derived from the above-mentioned reduced-order models. To ensure compatibility with the available measurements and improve structural observability, two modifications (with respect to the AM2HN model version) were introduced: (i) the states related to inorganic carbon (C) and total alkalinity (Z) were reformulated into the aggregated variable $\xi = Z - C$; and (ii) an additional state variable ($x_{M,gb}$) was introduced to represent the methane fraction (x_M) dynamics in the gasbag (subscript gb), thereby accounting for the plant hydraulics of the experimental setup (see Section 2.2). Indeed, the gasbag introduced a buffering effect, resulting in a measurable lag between the instantaneous and measured biogas composition. The resulting model (hereafter referred to as $AM2HN_{obs}$) has state vector $\mathbf{x} \in \mathbb{R}^{m+6}$ comprising: the particulate biodegradable fraction of each co-feedstock $\mathbf{X_h} \in \mathbb{R}^m$ ($g_{VS}\ L^{-1}$), the core AM2 states S_1 (biodegradable soluble COD), S_2 (TVFA), X_1 (acidogens biomass), X_2 (methanogens biomass), ξ (mmol L^{-1}), and $x_{M,gb}$. The input vector $\mathbf{u} \in \mathbb{R}^m$ contains the co-feedstock flow rates (L d^{-1}). The *online*-measurable outputs $\mathbf{y} \in \mathbb{R}^3$ are restricted to the total biogas flow rate q_{TOT} and its composition ($x_{M,gb}$, $x_{C,gb}$), consistently with industrial practice.

The structural observability of the model was assessed using a nonlinear geometric approach implemented in the *STRIKE_GOLDD* toolbox (Díaz-Seoane et al., 2022), following the methodology of Hellmann et al. (2023). In particular, the Full Input-State-Parameter Observability (FISPO) and Observability Rank Condition with Direct Feedthrough (ORC-DF) algorithms were employed, both based on the symbolic computation of Lie derivatives.

The final model used in the control scheme is given by Eqs. (1)–(10).

$$\dot{\mathbf{X}}_\mathbf{h} = D(\mathbf{X_{h,in}} - \boldsymbol{\alpha}\mathbf{X_h}) - \mathbf{k_h} \odot \mathbf{X_h} \tag{1}$$

$$\dot{X}_1 = (\mu_1 - \alpha D - k_{d,1})X_1 \tag{2}$$

$$\dot{X}_2 = (\mu_2 - \alpha D - k_{d,2})X_2 \tag{3}$$

$$\dot{S}_1 = D(S_{1,in} - S_1) - k_1\mu_1 X_1 + + \sum_{i=1}^{m}(COD_{X_h}/VS_{X_h})_i k_{h,i} X_{h,i} \tag{4}$$

$$\dot{S}_2 = D(S_{2,in} - S_2) + k_2\mu_1 X_1 - k_3\mu_2 X_2 \tag{5}$$

$$\dot{\xi} = \dot{Z} - \dot{C} = D(\xi_{in} - \xi) + \sum_{i=1}^{m} N_{X_{h,i}} k_{h,i} X_{h,i} - - N_x[(\mu_1 - k_{d,1})X_1 + (\mu_2 - k_{d,2})X_2] - - k_4\mu_1 X_1 - k_5\mu_2 X_2 + q_C \tag{6}$$

$$\dot{x_{M,gb}} = \frac{VRT}{1 \times 10^3 V_{gb} P_{tot}}(q_M - (q_C + q_M)x_{M,gb}) \tag{7}$$

$$y_1 = q_C + q_M = q_{TOT} \tag{8}$$

$$y_2 = x_{M,gb} \tag{9}$$

$$y_3 = x_{C,gb} = 1 - x_{M,gb} \tag{10}$$

where:

$$D = \frac{\sum_{i=1}^{m} u_i}{V} \tag{11}$$

$$\mu_1 = \mu_{max,1}\frac{S_1}{S_1 + K_{S,1}} \tag{12}$$

$$\mu_2 = \mu_{max,2}\frac{S_2}{S_2 + K_{S,2} + \frac{S_2^2}{K_{I,2}}} \tag{13}$$

$$CO_2 = S_2 - \xi \tag{14}$$

$$q_M = k_6\mu_2 X_2 \tag{15}$$

$$q_{M,gb} = x_{M,gb} q_{TOT} \tag{16}$$

$$\phi = CO_2 + k_H P_{tot} + \frac{q_M}{k_L a} \tag{17}$$

$$P_c = \frac{\phi - \sqrt{\phi^2 - 4k_H P_{tot} CO_2}}{2k_H} \tag{18}$$

$$q_C = k_L a(CO_2 - k_H P_c) \tag{19}$$

$$x_{in}^{(j)} = \frac{\sum_{i=1}^{m} u_i \theta_{in,i}^{(j)}}{\sum_{i=1}^{m} u_i}, \qquad j \in \{S_1, S_2, Z, C\} \tag{20}$$

$$\xi_{in} = Z_{in} - C_{in} \tag{21}$$

$$\mathbf{X_{h,in}} = \frac{\mathbf{u} \odot \mathbf{BD_{vs_p}} \odot \mathbf{VS_p}}{\sum_{i=1}^{m} u_i} \tag{22}$$

The vectors $\mathbf{BD_{VS_p}}$, $\mathbf{VS_p}$, $\mathbf{N_{X_h}}$ and $\mathbf{COD_{X_h}/VS_{X_h}}$ are derived from feedstocks' characterization. The influent composition is obtained as a flow-weighted average of the individual co-feedstocks (Eq. (20)). Unit density is assumed for all streams. Further details are provided in Sections II.B and II.C of the SM.

In the following, the percentage Mean Absolute Relative Error ($MARE_\%$) and the Pearson's coefficient of determination (r^2) were used as metrics to quantify the models' performances. The $MARE_\%$ expression is reported in Eq. (23), which holds for each measurable output $\tilde{y}$ observed for $N_{\tilde{y}}$ time data points.

$$MARE_\% = \frac{100}{N_{\tilde{y}}}\sum_{t=0}^{N_{\tilde{y}}}\left|\frac{y_t - \tilde{y}_t}{\tilde{y}_t}\right| \tag{23}$$

Practical observability was assessed by linearizing the model around the operating point and analyzing the resulting Jacobians through the Kalman observability matrix ($\mathcal{O}$) and the associated Gramian ($\mathbf{W}_\mathcal{O}$); the condition number of $\mathbf{W}_\mathcal{O}$ was used to quantify numerical conditioning,

while its inverse was examined to identify state confounding, i.e., situations in which multiple states exhibit indistinguishable effects on the measured outputs.

3.2. State observer design

The AM2HN$_{obs}$ model was used to design a discrete-time Extended Kalman Filter (EKF) (Dan, 2006). The model was discretized using a forward-Euler scheme with integration step Δt, and the EKF relies on the linearization of the state-transition and observation equations (Jacobian matrices computed via finite differences) to recursively estimate the states $\hat{\mathbf{x}}$ and their covariance $\mathbf{P}$, based on the process and measurement noise covariances $\mathbf{Q}$ and $\mathbf{R}$. The complete filter formulation is reported in Section II.E of the SM.

$\mathbf{Q}$ and $\mathbf{R}$ were assumed diagonal. The $\mathbf{R}$ was selected based on sensor accuracy and measurement quality, while the $\mathbf{Q}$ was tuned to reflect confidence in the model structure and *offline*-identified parameters, thereby balancing model prediction and measurement correction. The initial $\mathbf{P}$ was set with relatively large diagonal entries to account for the limited confidence in the initial state estimates ($\hat{\mathbf{x}}_0$), particularly for unmeasured states initialized from open-loop model predictions.

The EKF tuning, prior to real-time deployment, was performed through a structured combination of preliminary tests, Monte Carlo (MC) analyses, and validation on previously collected experimental data. First, preliminary tests (including +50% input steps and free responses) were conducted under the assumption of near-perfect model knowledge, i.e. almost-null $\mathbf{Q}$ and $\mathbf{R} = \text{diag}(\sigma_{\tilde{\mathbf{y}}}^2)$, where $\sigma_{\tilde{\mathbf{y}}}$ contains the standard deviation of the measurements (computed as the element-wise multiplication between each outputs' relative standard deviation ($\epsilon_{\tilde{\mathbf{y}}}$) and its time-average value ($\bar{\tilde{\mathbf{y}}}$)) and Gaussian measurement noise. A MC analysis was carried out on the initial state estimates, sampled via Latin Hypercube Sampling (LHS) within ±50% of $\hat{\mathbf{x}}_0$ (except ±9% for $x_{M,gb}$).

Uncertainties were introduced in both $\hat{\mathbf{x}}_0$ and the most uncertain kinetic parameters ($\boldsymbol{\theta_{kin}} \subset \boldsymbol{\theta_P} = \{K_{I,2}, K_{S,1}, K_{S,2}, \mu_{max,1}, \mu_{max,2}\}$), within ±20% of their nominal (*offline*-estimated) values. These perturbations were initially fixed to explore the **Q**-**R** design space. Finally, a robustness analysis was conducted on the selected **Q**-**R** configuration by propagating 400 MC simulations with perturbed $\hat{\mathbf{x}}_0$ and $\boldsymbol{\theta_{kin}}$ values. The convergence performance was quantified in terms of MARE$_{\%}$, r^2, and Mean Absolute Error (MAE, computed as MARE without normalization and multiplication by 100) with respect to the true states.

The resulting EKF design was validated on previously collected experimental data and iteratively fine-tuned to ensure satisfactory performance. A subsequent manual refinement led to the final configuration adopted for real-time implementation. The EKF performance, together with the multi-step ahead prediction accuracy (with *multi* equal to the number of integration steps required to propagate the open-loop model from the EKF estimates to cover one control interval without intermediate correction), was evaluated using the same metrics adopted for the open-loop models, i.e., MARE$_{\%}$ and r^2.

3.3. Control objectives

The control objectives were to (i) maximize biomethane production (q_M) while (ii) ensuring safe operation by keeping key variables within predefined bounds. Since TVFA concentration is not available *online*, the biogas composition ratio ($x_{C,gb}/x_{M,gb}$) was adopted as a reliable and low-cost *online*-available proxy, more informative than the *offline*-available FOS/TAC (Carecci et al., 2024a).

The agri-AcoDM model was used to perform a constrained *offline* optimization of the feeding strategy, defining time-varying setpoints $\mathbf{y_{ref}} = \{q_{M,gb,ref}, (x_{C,gb}/x_{M,gb})_{ref}\}$ and corresponding reference inputs $\mathbf{u_{ref}}$ to move from the initial sub-optimal to the final optimized diet/working condition. The optimization was subject to process constraints (e.g. D, TVFA and total COD limits) and input constraints (transition between initial and optimal diets over a 2-week ramp).

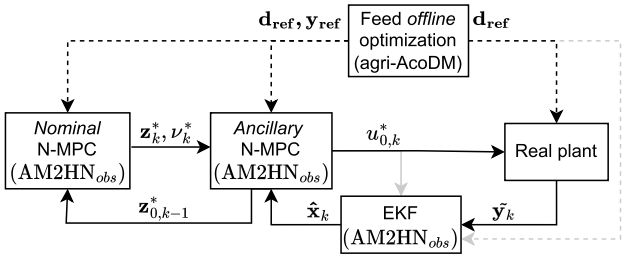

Fig. 3. Block diagram (contextualized to the case-study described in Section 2.3) of the tube-based NMPC control scheme (*online* formulation).

For real-time control, the robust tube-based NMPC formulation proposed in Carecci et al. (2025a) was adopted (Fig. 3). This approach relies on a decomposition of the control problem into a *nominal* (undisturbed) and an *ancillary* (disturbed) one: the latter, acting on the real system with states $\mathbf{x}$ and inputs $\mathbf{u}$, tracks the optimal trajectories computed for the nominal system ($\mathbf{z}$, ν), thus providing additional feedback compensation. The *online* formulation was specifically designed to cope with model uncertainty (e.g., $\boldsymbol{\theta_{kin}}$), disturbances, and partial state availability by recursively updating the nominal trajectories. This is achieved by introducing the initial nominal state $\mathbf{z}_0^*$ as a decision variable in the ancillary problem and enforcing consistency with the nominal prediction at the next k^{th} control step. The AM2HN$_{obs}$ model was used to describe the system dynamics and enforce state constraints. The feasible sets of the nominal ($\mathbb{Z}$) and ancillary ($\mathbb{X}$) problems were designed based on prior simulations and process knowledge to guarantee safe operation through constraint tightening ($\mathbb{Z} \subseteq \mathbb{X}$).

In parallel, a selector-PI controller, already validated in a comparable application (Carecci et al., 2024a), was implemented as a reference strategy to enable a qualitative comparison with a different control approach. It is noted that the objective of this comparison is not to establish strict superiority in tracking performance, but rather to assess the practical behavior of the two controllers under representative experimental conditions, within the limitations of the bench-scale setup, and in light of their inherently different control philosophies.

Further details about the control law formulations and parameters are reported in Sections II.F–G of the SM, as well as in the original manuscripts (Carecci et al., 2024a, 2025a).

3.4. Practical control implementation

As a result of the aforementioned actuation constraints in the bench-scale plant, the tomato sauce flow rate was the sole scalar feedback action u computed by the controllers ($m = 1$), while the impulsive manual feeding of maize silage and cow slurry was treated as known (and significant) disturbances $\mathbf{d} \in \mathbb{R}^2$ ($\mathbf{d}_{\text{ref}}$ in the case of the feeding schedule suggested by the *offline* diet optimization). This reduced the control problem from a multiple-input multiple-output (MIMO) to a single-input multiple-output (SIMO) configuration (see Fig. 3 and Fig. 4). Together with the aforementioned continuity limitation of gas composition analysis (resulting in a sampling frequency of approximately 4 measurements per day on average), the controllers were therefore validated under representative yet challenging/non-ideal experimental conditions, so that satisfactory performance at laboratory scale can be regarded as a conservative estimate of the achievable performance in industrial implementations. The modeling and control framework was implemented using a combination of open-source software. The high-fidelity agri-AcoDM model was developed in OpenModelica (using the Modelica language), while the reduced-order model, EKF, and controllers were implemented in Python using the SciPy and CasADi libraries. The discrete integration step Δt was set equal to 5 min (and the pulses of $\mathbf{d_{ref}}$ approximated accordingly). The *offline* optimization problems were solved via

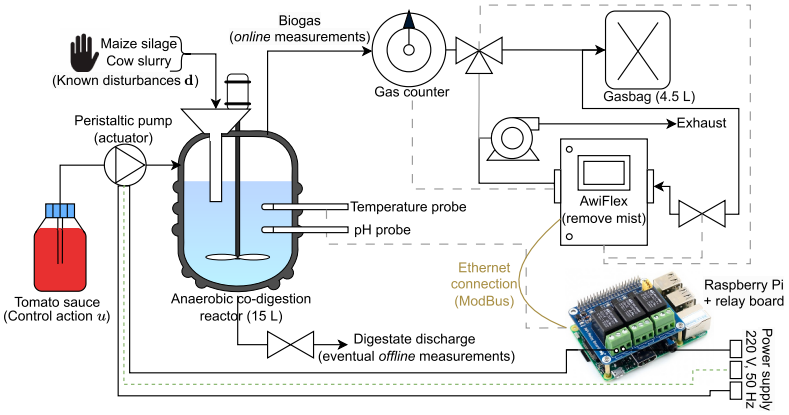

Fig. 4. Scheme of the closed-loop architecture as practically implemented around the bench-scale plant.

Differential Evolution algorithm (with a final refinement via Nelder-Mead iterations), whereas the *online* NMPC problems were solved using the Interior Point OPTimizer (IPOPT).

Data acquisition and control were handled through a local embedded platform, enabling real-time communication with the control algorithms, and actuation was via peristaltic pumps driven by a Raspberry Pi-based GPIO relay board. At each control step, the scalar control action u was mapped to a pulse-width-modulated (PWM) signal, in which the duty cycle determined the ON/OFF switching times of the relay. Control intervals (T_c) were selected based on process dynamics (typically 2-12 h, considering gas-phase and TVFA responses).

Basic data preprocessing and synchronization strategies were applied to ensure consistency between measurements and control updates. It is important to stress that the full-scale applicability of the proposed methodology relies on the *online*-availability of biogas flow rate and composition only. Indeed, the other variables measured *offline* were not available at a frequency compatible with T_c and were therefore used solely for monitoring and a posteriori validation.

The values of $\epsilon_{\bar{y}}$ were set from realistic sensor noises levels (assuming constant relative measurement errors of 5% for the biogas flow rate and 3% for the gas compositions).

In closed-loop operation, the tube-based NMPC execution time was approximately 10 min per control step, thus well below the adopted T_c.

Further practical implementation details are provided in Section II.H of the SM.

4. Numerical results

4.1. Models performance and limitations

Detailed methods and results for the *offline* parameter estimation of both high-fidelity and reduced-order models are reported in a previous work (Carecci et al., 2025b). In that study, a highly informative experimental dataset, collected during the experiment described by Carecci et al. (2024a) (similar feedstocks and operating conditions to the current experimentation), was used to train and validate the agri-AcoDM, yielding satisfactory accuracy in reproducing the main process variables. Subsequently, the reduced-order model parameters were estimated in two stages: (i) initial training on highly informative synthetic data generated by the agri-AcoDM, and (ii) refinement of only the practically identifiable parameters (identified according to the method proposed by Brun et al., 2001) using a subset of the above-mentioned real data (Carecci et al., 2025b). Because the resulting AM2HN model showed adequate performance relative to both agri-AcoDM and experimental data, the same parameter values were adopted for the AM2HN$_{obs}$ model version and are reported in Table S2 of the SM.

Despite their overall satisfactory performance, all the aforementioned models showed limited ability to capture the onset of a temporary VFA (mainly acetate) accumulation occurring during the *transient* from a sub-optimal to an optimized diet (under an experiment design similar to the one considered in this work; see Fig. 6), as extensively discussed in previous works (Carecci et al., 2025b). Capturing this type of incipient inhibition is of primary importance for developing a reliable model-based controller. This discrepancy is likely attributable to errors in state and/or parameter values, which can in principle be compensated through state observers and/or recursive parameter estimation algorithms (see Section 5.3 for further comments). Since the majority of the AM2HN$_{obs}$ states are not measurable *online* in practice, the logical next step toward MPC was the design of a suitable state observer.

4.2. Structural observability analysis

The structural observability analysis of the AM2HN$_{\text{tan}}$ model revealed a rank deficiency of 2 states, and, in particular, the additional TAN state as not-observable when only gas-phase measurements are available. Given that the investigated case study involves highly buffered digesters, with no N-rich feedstock used as a manipulated input, and considering the satisfactory predictive performance of the AM2HN model, TAN prediction was therefore omitted in favor of predictors with improved observability properties.

Further analysis of AM2HN showed that the simultaneous presence of states Z and C causes the main observability limitation (rank deficiency of 1 state) that characterizes the original AM2 model as well, thus complementing the findings reported by Attar and Haugen (2018). The intuition to guarantee full rank was to substitute such quantities with a new state variable ξ, computed as their difference (Eq. (6)). This reformulation reduces the pH predictability. However, in highly buffered digesters, pH fluctuations are attenuated, and VFA accumulation generally precedes inhibition effects associated with low pH. Consequently, this loss was considered acceptable provided that full-rank observability was met.

The inclusion of gasbag dynamics did not impair observability, although it increased the required Lie-derivative order from 3 to 4. Full observability was retained for configurations with up to $m = 4$ co-feedstocks.

The resulting AM2HN$_{obs}$ model was found to be locally structurally observable using gas-phase measurements only.

4.3. EKF validation

Considering the best tentative design of the EKF found from the preliminary tests described in Section 3.2, Fig. 5 shows the results of the robustness analysis to uncertain $\hat{\mathbf{x}}_0$ and $\boldsymbol{\theta}_{\boldsymbol{kin}}$ variations. The convergence

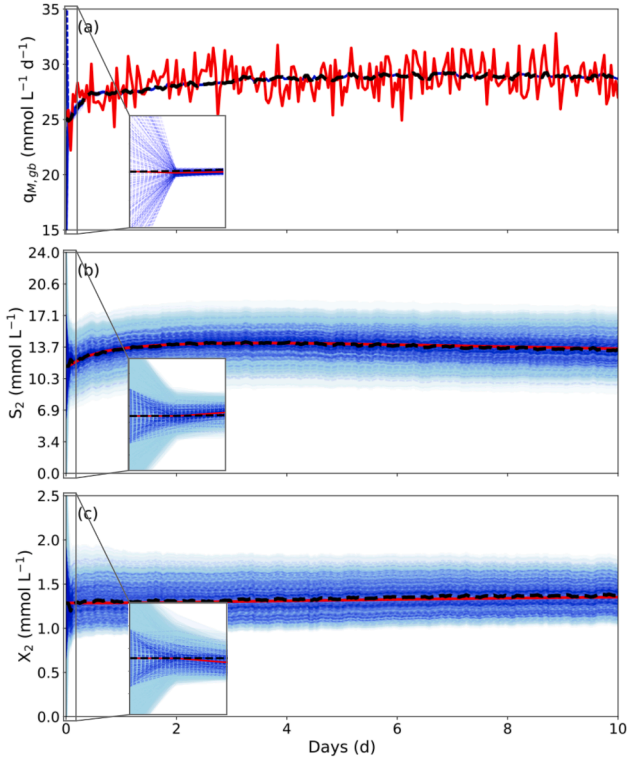

Fig. 5. EKF MC robustness analysis to $\hat{\mathbf{x}}_0$ and $\boldsymbol{\theta}_{kin}$ uncertainties (step response). (a) Biomethane flow rate; (b) TVFA concentration; (c) Methanogens concentration. True state/output (red line) against estimated state/output (dashed blue lines) and relative 95% confidence interval (light-blue filling). The black dashed line is the average of all the trajectories estimated by the EKF.

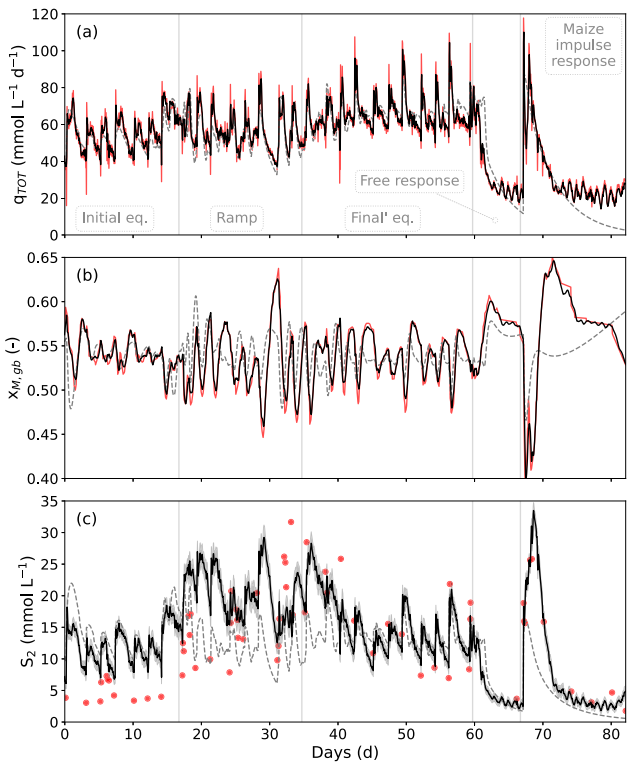

Fig. 6. EKF validation data collected from the experiment described in Carecci et al. (2024a). (a) Biogas flow rate; (b) Methane fraction in the biogas; (c) TVFA concentration. Data (red) vs open-loop AM2HN$_{obs}$ model (dashed gray line), and EKF estimation (black) with its relative 95% confidence interval (gray shading).

performance of the ensemble of system trajectories was quantified in terms of the average and standard deviation over the 400 MC runs of the MARE$_{\%}$, MAE, and r^2 with respect to the true states (values reported in Section III of the SM, Table S10). Although a persistent offset, due to the high collinearity between certain states and parameters, was present for the majority of the cases, the estimation error was considered acceptable especially for key states (e.g. $\overline{\text{MARE}}_{\%} = 6 \pm 4$ for S_2), and the trends were generally well captured (e.g., $\bar{r}^2$ amounts to 0.7–0.8 $\pm$ 0.2 for S_2 and X_2). It is also interesting to note that: (i) the major deviations occurred for S_1 and X_1, due to the high collinearity and poor practical observability of the faster kinetics related to the acidogenic step; (ii) the $\overline{\text{MAE}}$ and σ_{MAE} of S_2 and ξ were almost the same, reflecting their collinearity in the expression of CO_2 (see Eq. (14)). Moreover, the EKF exhibits relatively rapid convergence, with most of the transient vanishing within approximately 2 h (recall $\Delta t = 5$ min), as evidenced by the zoomed views in Fig. 5.

Additional discussion on practical observability (including collinearity effects) is presented in Section 5.3.

Before the experimental campaign of the current work, a validation of the estimation capabilities of the proposed EKF design was carried out over the past data collected from the experiment described in Carecci et al. (2024a). Starting from the previously obtained EKF design, trial-and-error adjustments were made to find a combination that both filters the measurement noise and provides satisfactory S_2 estimates compared to *offline* experimental data, thereby improving the open-loop predictions (model correction). The resulting **Q** and **R** values are reported in Table 1, and Fig. 6 shows the performances obtained with that design: compared to the open-loop AM2HN$_{obs}$ model, the EKF strongly improved the matching of the gas data, and, coherently with the experimental observations, it reproduced the temporary accumulation of TVFA (from day 14 to day 42) over the diet *transient* period that even

Table 1
Square-root diagonal entries of the AM2HN$_{obs}$-based EKF **Q** and **R** matrices. Values obtained from the validation over the data of the experiment described in Carecci et al. (2024a) (first column), and used in real-time for the experiment addressed in this work (second column). The '(1)' index stands for maize silage, '(2)' for cow slurry and '(3)' for tomato sauce.

	diag(Q)$^{0.5*}$ (Carecci et al., 2024a)	diag(Q)$^{0.5}$ [this work]
$X_h^{(1)}$ (g$_{VS}$ L^{-1})	3.78e^{-3}	7.00e^{-3}
$X_h^{(2)}$ (g$_{VS}$ L^{-1})	3.78e^{-3}	6.23e^{-3}
$X_h^{(3)}$ (g$_{VS}$ L^{-1})	3.78e^{-3}	3.01e^{-3}
X_1 (g$_{VS}$ L^{-1})	3.78e^{-3}	1.96e^{-3}
X_2 (g$_{VS}$ L^{-1})	3.78e^{-3}	3.57e^{-3}
S_1 (g$_{COD}$ L^{-1})	3.78e^{-3}	4.15e^{-4}
S_2 (mmol L^{-1})	3.78e^{-3}	2.67e^{-2}
ξ (mmol L^{-1})	3.78e^{-3}	1.43e^{-2}
$x_{M,gb}$ (-)	1.00e^{-4}**	7.36e^{-5}
	diag(R)$^{0.5***}$ (Carecci et al., 2024a)	*diag*(R)$^{0.5}$ [this work]
q_{TOT} (mmol L^{-1} d^{-1})	4.80	3.10
$x_{M,gb}$ (-)	2.70e^{-2}	4.28e^{-2}
$x_{C,gb}$ (-)	1.63e^{-2}	3.79e^{-2}

*$diag(\mathbf{Q})_{ub}^{0.5} = \mathbf{1.00e^{-2}}$; $diag(\mathbf{Q})_{lb}^{0.5} = \mathbf{1.00e^{-3}}$; **fixed
***$diag(\mathbf{R})_{ub}^{0.5}$ = [19.0, 3.16e^{-2}, 3.16e^{-2}];
$diag(\mathbf{R})_{lb}^{0.5}$ = [2.45, 6.78e^{-3}, 6.78e^{-3}]

the open-loop agri-AcoDM was not able to catch. Indeed, the S_2 MARE$_{\%}$ was reduced by 15% and r^2 doubled. This result was a key prerequisite for model-based control, in which reliable detection of incipient instabilities via state estimation is essential for effective closed-loop operation.

4.4. Closed-loop simulation

Early numerical assessment and tuning of the tube-NMPC closed-loop strategy was carried out in Carecci et al. (2025a), using a reactor

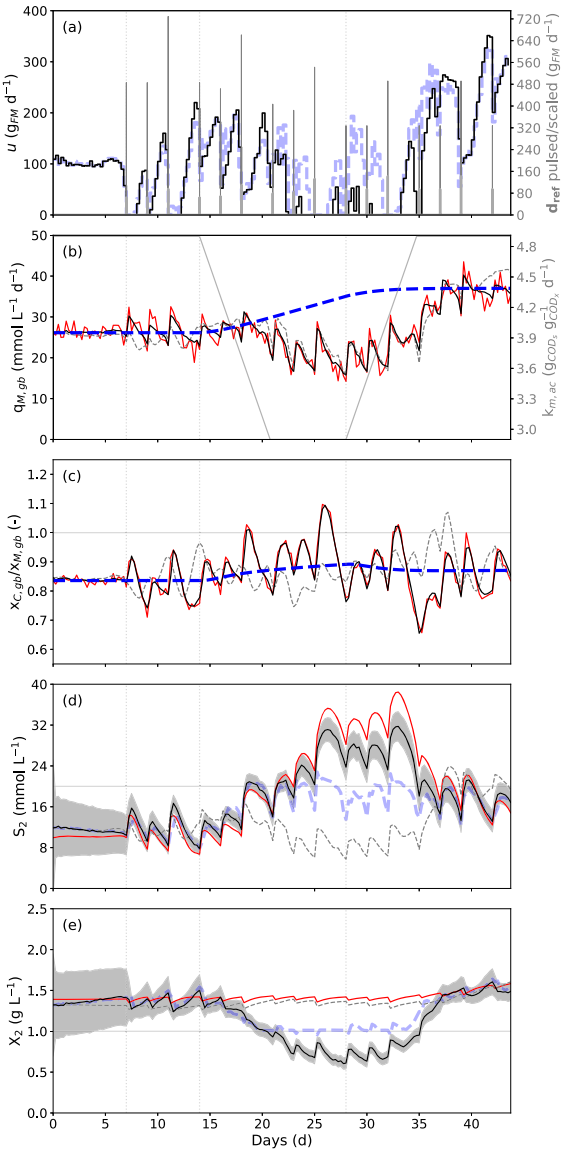

Fig. 7. Simulation (seed = 0) results of the combined EKF and *online*-tube NMPC. (a) Input flow rate; (b) Biomethane flow rate; (c) CO_2/CH_4 biogas ratio; (d) TVFA concentration; (e) Methanogens concentration. The secondary y-axis in (a) reports the daily pulsed feeding moments of $\mathbf{d}_{\mathbf{ref}}$, i.e., maize silage (thicker line) and cow slurry. The secondary y-axis in (b) reports the temporary reduction of the $k_{m,ac}$ imposed in the real reactor. Actual state/output (red) versus open-loop AM2HN$_{obs}$ model (gray dashed line) and EKF estimation (black) with its relative 95% confidence interval (gray shading). $\mathbf{y}_{\mathbf{ref}}$ as blue dashed line; $\mathbf{z}^*$ and v^* as light-blue dashed lines. $\mathbf{z}$ bounds as gray horizontal lines; start of the pulsed $\mathbf{d}_{\mathbf{ref}}$ and start-end of the ramp between initial and final equilibrium as gray dotted vertical lines.

simulated with the agri-AcoDM model and assuming full state measurement (i.e., without observer). It should be noted that the realistic simulations examined in prior work already accounted for these feeding and actuation conditions (Carecci et al., 2025a). The tracking and robustness of the controller were assessed using the MARE$_{\%}$ with respect to $\mathbf{y}_{\mathbf{ref}}$ and the maximum values of the measured stability proxies (i.e. $x_{C,gb}/x_{M,gb}$ and $\tilde{S}_2$), respectively.

Similar results were obtained when combining the tube-NMPC with the EKF described in Section 4.3. Since state trajectories remained well within their bounds, the daily-averaged control action u closely followed the profile suggested by the *offline* optimization (u_{ref}), yielding near-perfect tracking of $q_{M,gb,ref}$. This behavior can likely be attributed to (i) the use of the same agri-AcoDM model for both computing the optimal diet (and the resulting control setpoints) and emulating the plant, and (ii) the low average EKF estimation errors (MARE$_{\%} \approx$ 5–15% for all states), attributable to effective noise filtering and accurate AM2HN$_{obs}$ model training (Carecci et al., 2025b).

Subsequently, as in the simulation study of Since the fixed-parameter agri-AcoDM model was unable to capture such dynamics (Section 4.1), this was achieved by temporarily reducing $k_{m,ac}$ during the *transient* period, acting as an unknown disturbance to the controller. The simulation was repeated 30 times with different $k_{m,ac}$ realizations (MC analysis), and one representative run is shown in Fig. 7.

Overall, the EKF-NMPC combination effectively rejected the unknown $k_{m,ac}$ disturbance during the *transient* period, preventing the process failure that would have occurred without control (Carecci et al., 2025a). It is interesting to examine the key dynamics shown in Fig. 7 that underlie this performance, and how the EKF estimation errors (MARE$_{\%}$ = 13.8% for S_2) influenced the NMPC decisions. During the initial equilibrium phase (days 7–14), the switch to impulse feeding accelerated EKF convergence, and estimation offsets remained modest (5–15%). As a result, $q_{M,gb,ref}$ tracking was near-perfect over this period. During the *transient* phase (days 14–28), the $k_{m,ac}$ disturbance caused $\tilde{S}_2$ to rise in the simulated real digester. Since the endogenous EKF could not re-estimate process parameters *online*, it compensated for the modeling mismatch in $x_{C,gb}/x_{M,gb}$ by overestimating $\hat{S}_2$ and underestimating $\hat{X}_2$, relative to open-loop trajectories, effectively mimicking a time-varying $\mu_{max,2}$ (the AM2HN$_{obs}$ analog of $k_{m,ac}$). In response, the NMPC reduced the OLR to saturation at zero tomato sauce load to keep S_2 and $x_{M,gb}$ within their bounds, at the cost of inaccurate $q_{M,gb,ref}$ tracking. Once the disturbance subsided (day 35 onward), $\tilde{S}_2$ recovered below its upper bound, and the controller progressively restored and increased the OLR to match the final equilibrium's $q_{M,gb,ref}$. Compared to Carecci et al. (2025a), similar performances were obtained in terms of $q_{M,gb,ref}$ tracking, yet with slightly lower stability of the *transient* operations ($\tilde{S}_{2,max} \approx 40$ instead of ≈ 32 mmol L^{-1}).

These results highlighted two key design requirements: (i) the *online* measurability of $x_{C,gb}/x_{M,gb}$ is essential for the EKF to track VFA accumulations not captured by the open-loop model; (ii) a robustness-oriented tightening of the stability-proxies constraints is required to enable timely counteraction of emerging instabilities.

5. Experimental results

5.1. Closed-loop validation

After the minor adaptations of the models to the specific co-feedstocks and operating conditions of the experimental campaign addressed in this work (e.g., influent composition, minor manual adjustment of k_La), the agri-AcoDM was used to perform the *offline* optimization of the diet: the results in terms of the main process characteristics of both the initial sub-optimal and final optimized equilibrium are reported in Table 2. The $\mathbf{y}_{\mathbf{ref}}$ and related $\mathbf{d}_{\mathbf{ref}}$ trajectories to be imposed to the reactors were thus defined: whereas $q_{M,gb}$ ramps monotonically, both TVFA and CO_2/CH_4 trajectories increase and peak during the *transient* between the two steady-states and then decrease back to similar values to those of the initial equilibrium (the actual setpoint trajectories used during closed-loop operations are depicted in Fig. 9).

Further refinement/re-tuning of the AM2HN$_{obs}$ model parameter values before closed-loop operations was not conducted, since only gas data were available in the first weeks of the experimental campaign (the first TVFA data were made available with substantial delays due to equipment limitations), and thus the dataset was poorly informative. Since the open-loop model performance over the same period was deemed satisfactory (see Fig. 9 and Section III.A of the SM), it was decided to proceed accordingly, thereby allowing the whole dataset from the current experiment to be fully exploited for model validation (see Section 5.3).

Table 2
Process characteristics of the initial and final equilibrium (the latter as found by the *offline* optimization carried out with the agri-AcoDM model).

	Initial eq.	Final eq.
HRT (d)	31.74	32.36
OLR (g_{COD} L^{-1} d^{-1})	2.89	3.76
Maize silage* (g d^{-1}) [$\%_{OLR}$]	39 [45%]	62 [58%]
Cow slurry* (g d^{-1}) [$\%_{OLR}$]	240 [26%]	197 [17%]
Tomato sauce** (g d^{-1}) [$\%_{OLR}$]	100 [29%]	111 [25%]
$q_{M,gb}$ (mmol L^{-1} d^{-1})	28.55	38.14
CO_2/CH_4 (-)	0.885	0.900
TVFA (mmol L^{-1})	12.12	12.23
Total COD (g_{COD} L^{-1})	39.5	47.9
TAN (g_N L^{-1})	1.12	0.952
pH (-)	7.41	7.13

**search space within [−30,100] and [-80,100], respectively (on fresh-matter basis).*
***search space within [−95, 200] (on fresh-matter basis).*

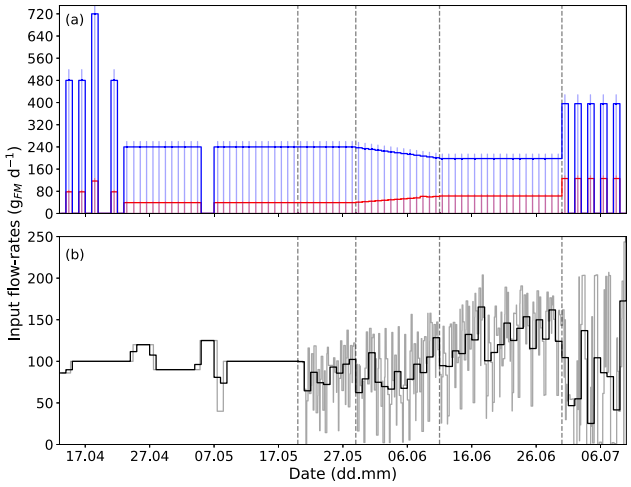

Fig. 8. Daily loads of the actual experiment. In (a): $\mathbf{d}_{\mathbf{ref}}$ loads of maize silage (red) and cow slurry (blue). Exact feeding instants correspond to clearer, continuous vertical lines. In (b): tomato sauce dosages requested to the pumps of the 'NMPC' reactor (closed-loop control actions from 20/05/2025). Vertical dashed gray lines report the start of the closed-loop phase, start and end of the ramping period, and the start of the final period with $\mathbf{d}_{\mathbf{ref}}$ feeding every 2 days. An acetate pulse was applied on 05/05/2025.

Using the **Q** and **R** parameterization from Section 4.3, a final manual fine-tuning of the EKF was carried out, based on the data collected over the same aforementioned time period before real-time closed-loop operations (Table 1, see Section 5.3 for further details). A temporary TVFA increase observed between 15–27/04/2025 (during late start-up phase, symptomatic of methanogenic inhibition), served as a final validation of the EKF design: $\text{diag}(P)^{(S_2)}$ increased and $\hat{S}_2$ tracked the experimental TVFA trend, consistently with simulation results, albeit with a residual offset (≈ 27%, see Fig. 9). The manual feeding frequency of **d** was accordingly modified from 3 times per week to daily on 23/04/2025, to mitigate the inhibition by reducing the magnitude of the load pulses.

Accordingly, compared to the previously conducted simulations studies, few settings of the experimental closed-loop operation differed (e.g., $S_{2,ub} = 15$ instead of 20 mmol L^{-1}, daily feeding frequency of $\mathbf{d}_{\mathbf{ref}}$ instead of 3 times per week) and are summarized in Section II of the SM. As previously stated, one reactor was controlled by the tube-based NMPC (labeled 'NMPC', see Fig. 3) and a second reactor by the selector-PI (labeled 'Selector-PI'). The remainder of this section is dedicated to the closed-loop 'NMPC' results, but further discussion on the 'Selector-PI' results and a concluding benchmarking analysis can be found in Section 5.2.

Fig. 8(a) shows the time evolution of both the actual known **d** (maize silage and cow slurry dosages; equal to $\mathbf{d}_{\mathbf{ref}}$ over the closed-loop period) fed manually, and Fig. 8(b) the tomato sauce dosages (control action u over the closed-loop period) requested before and during closed-loop operations (start on 20/05/2025), along with the daily averages. In the last days of the experiment (30/06–10/07/2025), the manual feeding frequency was reduced from daily to once every 2 days to challenge the controllers' behaviors under more demanding operating conditions. Fig. 9 reports the main output trajectories, along with the relative AM2HN_{obs} open-loop model predictions and EKF corrections/estimates. The tracking results are shown in Fig. 9a-b, and quantified in Table 3, whereas the comparison between the setpoints and the output's daily averages is reported in Fig. 10, for the sake of readability. The tracking was satisfactory, as highlighted by the $\text{MARE}_{\%}$ below 30% and 6% for $q_{M,gb}$ and $x_{C,gb}/x_{M,gb}$, respectively (8% and 4% if daily averages are considered). The actual average biomethane production during the final steady-state period (21–30/06) was only 6% lower than the expected optimal value. Overall, a stable increase of ≈ 17% in biomethane production was obtained under safe operations, compared to the ≈ 27%[1] predicted by the agri-AcoDM, while the average control action $\bar{u}$ requested to the pump differed by -14% and 24% over the initial and final periods, respectively. However, a small mismatch between the suggested control action and the actual dosage fed by the pump (computed as the difference in the weight of the tomato sauce storage bottle) was present (9% on average), mainly due to equipment limitations: overall, the final error in the specific biomethane production at the optimized final steady-state was ≈ 9.5% (272.7 instead of 299.0 NmL_{CH_4} g_{VS}^{-1}).[2] In the last days of the experiment, with halved feeding frequency of $\mathbf{d}_{\mathbf{ref}}$, the NMPC decreased significantly the control action and worsened the $q_{M,gb,ref}$ tracking due to the higher modeling mismatch (in the discharge phase of the impulse response) and predicted violations of both S_2 and $x_{C,gb}/x_{M,gb}$ constraints (over the peaks of the impulse responses).

Unlike in previous experimental evidence (Carecci et al., 2024a, 2025b), no inhibition occurred during the diet *transient*. It is worth recalling that the tube-NMPC was tuned with a robustness-oriented philosophy to ensure recursive feasibility and constraint satisfaction under bounded uncertainties, including the worst-case scenario of the possible occurrence of such *transient* inhibition (Carecci et al., 2025a) (Section 4.4). This was achieved through three design choices: (i) a high weight on nominal state trajectories ($w_x = 80\%$ of the terminal output cost weight $w_{y_{H_p}}$); (ii) inclusion of the stability proxy $(x_{C,gb}/x_{M,gb})_{ref}$ among the controlled outputs, with a weight of 80% of that on biomethane flow rate; and (iii) tight bounds on stability proxies S_2 and $x_{M,gb}$ (e.g. the upper bound on S_2 was set ≈ 30% below a reasonable expert-driven admissible value). Together, these choices induced a safe closed-loop dynamic behavior, which explains the observed ≈ 30% instantaneous biomethane flow rate tracking error (≈ 8% on daily averages), resulting from the inherent robustness/tracking trade-off of tube-based formulations, rather than inadequate tuning.

5.2. Controller benchmarking

A detailed comparison between the two controllers is provided in Section III.C of the SM.

[1] computed considering the time averages–during the initial and final periods–of the $q_{M,gb,ref}$ obtained simulating a daily (instead of a constant) feeding mode.
[2] computed dividing the average biomethane production by the average concentration of VS in the input diet, for both the actual and the agri-AcoDM-optimized values, respectively.

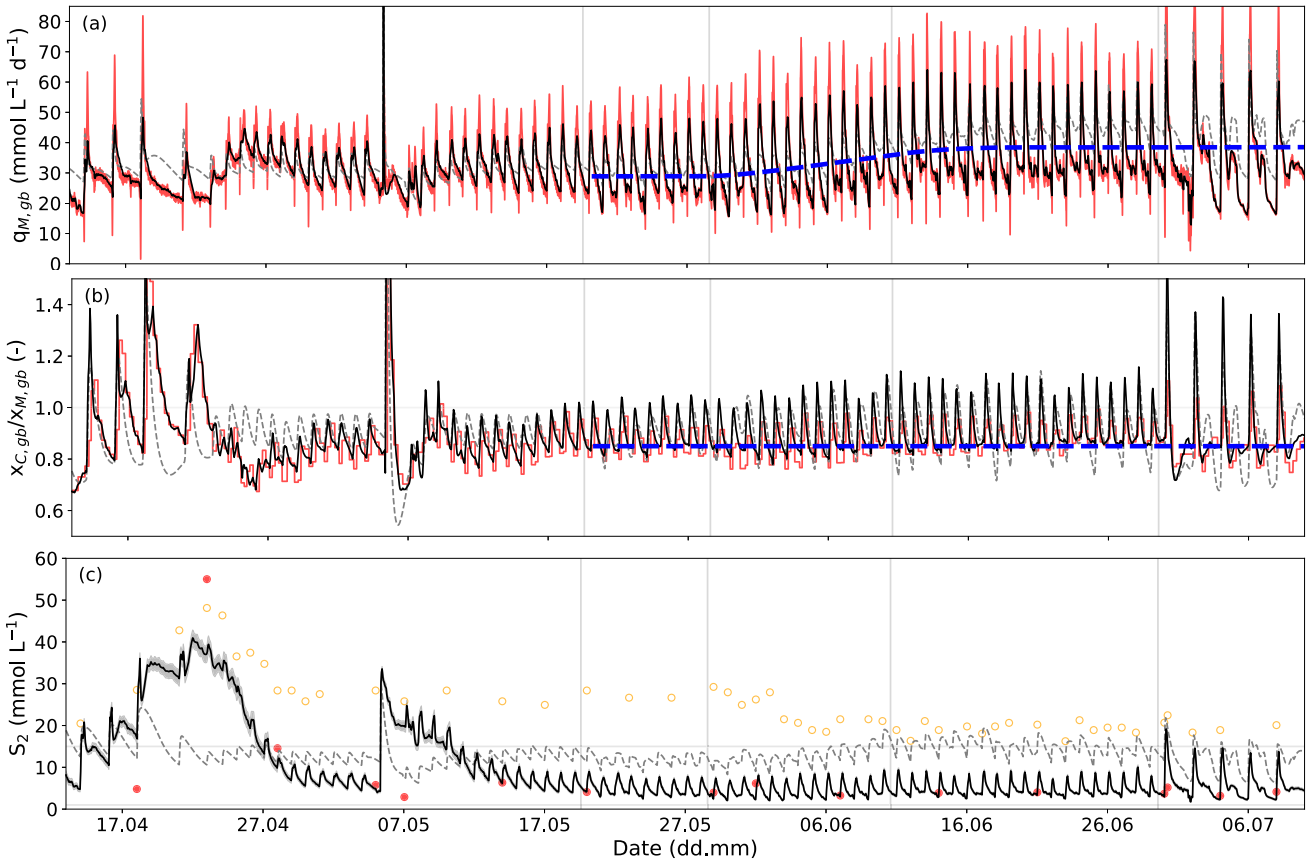

Fig. 9. Results of the real experiment for the reactor controlled by the NMPC. (a) Biomethane flow rate; (b) CO_2/CH_4 biogas composition ratio; (c) TVFA concentration. Data (red) against open-loop AM2HN$_{obs}$ model (gray dashed line) and EKF estimation (black) with its relative 95% confidence interval (gray filling). $\mathbf{y}_{\mathbf{ref}}$ as blue dashed lines, $\mathbf{z}$ bounds as horizontal gray lines and the above-mentioned "control periods" delimited by the vertical gray lines. In (c) the IA is also shown as empty circles with orange outline.

Table 3
Quantification/metrics of the 'NMPC' controller's performance.

	Time window*	Biomethane flow rate		Biogas composition ratio		*Controlaction* **
	(dd/mm – dd/mm)	$\mathbf{q}_{\mathbf{M,gb}}$ (mmol d^{-1} L^{-1})	MARE$_{\%}$	$\mathbf{x}_{\mathbf{C,gb}}/\bar{\bar{\mathbf{x}}}_{\mathbf{M,gb}}$ (–)	MARE$_{\%}$	$\bar{\mathbf{u}}$ (g_{FM} L^{-1})
'NMPC'	20/05 – 29/05	31.10	28.55	0.866	5.12	86.13 (92.15)
	21/06 – 30/06	36.25	26.78	0.889	5.45	138.0 (113.8)
	20/05 – 30/06	34.38	29.84	0.869	5.47	104.8 (96.92)

*20/05 – 29/05: initial equilibrium; 21/06 – 30/06: final equilibrium; 20/05 – 30/06: overall closed-loop period with daily feeding.
**the $\bar{u}$ value within brackets is the amount actually fed by the peristaltic pumps (net of actuation imperfections).

The tube-based NMPC achieved biomethane flow rate tracking comparable to the selector-PI (≈ -7%), while exhibiting smoother control actions and lower oscillations in stability-related indicators (e.g. ≈ -2.5% and -64% peak value of $x_{C,gb}/x_{M,gb}$ and TVFA respectively), consistent with its explicit constraint-handling and robustness-oriented design. Conversely, the selector-PI displayed a more pronounced bang–bang behavior with higher saturation liability, yielding slightly tighter instantaneous biomethane flow rate tracking and marginally higher specific methane production at the final equilibrium.

Given the intrinsic variability of the bioprocess, the practical constraints of bench-scale experimentation (manual feeding of TS-rich feedstocks, intermittent sensor continuity), and the absence of unstable operation during the diet *transient*, the small differences observed between the two reactors do not support statistically strong claims of superiority. However, the comparison is inherently asymmetric: the NMPC explicitly enforces an upper bound on TVFA, whereas the selector-PI does not; the observed differences therefore reflect distinct control philosophies rather than the superiority of one strategy.

Beyond tracking, the principal advantage of the NMPC lies in its model-based predictive structure, which enables systematic constraint handling, scenario analysis, and straightforward MIMO extension. These features become particularly relevant in full-scale applications, where high-frequency automated feeding of TS-rich feedstocks enables MIMO control and where multi-objective regulation is required (e.g., biomethane production, digestate quality, and diet composition). In addition, significant and unexpected inhibition events remain a realistic operational risk in full-scale applications, making the robustness-oriented design of NMPC particularly beneficial for maintaining safe operation and preventing process failure due to TVFA accumulation. Overall, the experimental campaign achieved its primary objective, namely the validation of the NMPC framework in real-time operation, although its advantages over the benchmark controller are expected to become more evident in full-scale and long-term industrial applications.

Table 4
Metrics of the open-loop models, EKF and multi-step ahead ($AM2HN_{obs}$) model's performances.

	Time window***	$\mathbf{q_M}$		$\mathbf{CO_2/CH_4}$		TVFA	
	(dd/mm – dd/mm)	$MARE_{\%}$	r^2	$MARE_{\%}$	r^2	$MARE_{\%}$	r^2
agri-AcoDM*	13/04 – 10/07	24.4	0.25	8.5	0.13	149.7	0.01
	20/05 – 30/06	27.4	0.22	5.6	0.17	182.1	0.15
Open-loop $AM2HN_{obs}$	13/04 – 10/07	27.4	0.27	10.4	0.14	144.0	0.00
	20/05 – 30/06	31.3	0.34**	7.4	0.41	175.5	0.29
EKF $AM2HN_{obs}$	13/04 – 10/07	7.3	0.90	6.7	0.48	86.3	0.62
	20/05 – 30/06	7.3	0.94	6.1	0.29	25.7	0.17
Multi-step ahead $AM2HN_{obs}$	13/04 – 10/07	18.4	0.47	6.4	0.32	41.5	0.06
	20/05 – 30/06	19.4	0.49	5.6	0.41	20.8	0.14

*see Section III of the SM for the results on other variables. **0.79 if daily averages are considered.
***13/04 – 10/07: overall experiment (after inoculum adaptation); 20/05 – 30/06: overall closed-loop period with daily feeding.

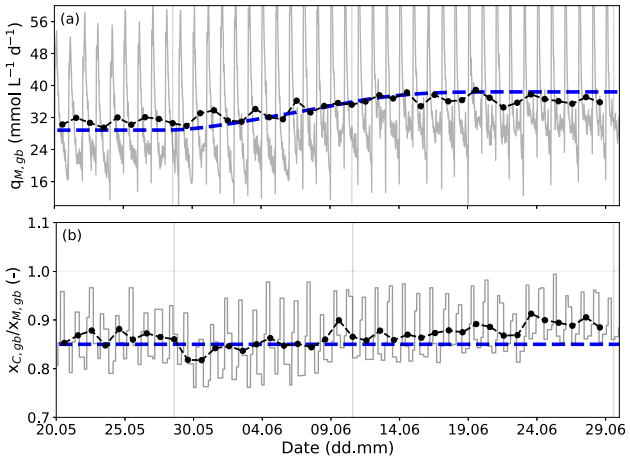

Fig. 10. Tracking of $\mathbf{y_{ref}}$ (black dashed lines) by the 'NMPC' over closed-loop operations. (a) Biomethane flow rate; (b) CO_2/CH_4 biogas composition ratio. Real data are shown as clearer lines, whereas the daily averages are shown as dashed thicker lines with markers.

5.3. Models and EKF performance

Models' performance metrics for the 'NMPC' reactor are reported in Table 4. The Figs. S2 and S3 present in Section III.A of the SM complement Fig. 9, reporting the open-loop performances of both agri-AcoDM and $AM2HN_{obs}$ models to show the consistency with the claims of Section 4.1 and previous works (Carecci et al., 2025b). Open-loop $MARE_{\%}$ remained below 31.3% and 12.6% for $q_{M,gb}$ and $x_{C,gb}/x_{M,gb}$ respectively (below 13.2% and 7.7% on daily averages, with r^2 up to 0.79). The agri-AcoDM outperformed $AM2HN_{obs}$ in terms of $MARE_{\%}$ (≈ 23% on average), but showed similar r^2. Notably, the $q_{M,gb}$ error was substantially lower at initial than at final equilibrium (from 20.1% to 39.7% and from 2.3% to 26.6% for instantaneous and daily-averaged $MARE_{\%}$).

The EKF effectively filtered measurement noise and corrected open-loop model outputs, reducing $MARE_{\%}$ below 4.4% and raising r^2 above 0.95 (on daily averages). Since the $AM2HN_{obs}$ model cannot capture the discrete event-based availability of gas composition data, the filter was intentionally tuned to avoid exact step-wise tracking of $x_{C,gb}/\tilde{x}_{M,gb}$, favoring physically consistent transient dynamics (e.g. the CO_2 peak shortly after pulsed feeding of C-rich feedstocks). Multi-step ahead predictions were satisfactory: on daily averages, $MARE_{\%}$ and r^2 remained below 4.7% and above 0.64, respectively, approximately twice better than the open-loop model.

Both open-loop models exhibited a systematic S_2 overestimation throughout the closed-loop experiment, resulting in amplified $MARE_{\%}$ (≈ 150%) due to the low absolute values of $\tilde{S}_2$, despite visually reasonable predictions (Fig. 9c). This offset likely reflects inaccurate $\mu_{max,2}$ and/or $K_{S,2}$ values for the specific microbial consortium that developed from the inoculum used in this experiment, compared to the one that grew during the previous experiment whose data were used for *offline* parameter estimation purposes, suggesting that re-tuning could improve TVFA predictions. Real-time recursive parameter update could have been an alternative (Carecci et al., 2025b), but its non-trivial integration with the EKF–due to different time scales of state and parameter variations and collinearity between certain states and parameters (X_2, S_2 and $\mu_{max,2}$ in the expression of q_M, Eq. (15))–was considered beyond the scope of this work. The EKF successfully compensated by reducing $\hat{S}_2$ (and consistently increasing $\hat{X}_2$), substantially improving $MARE_{\%}$ and r^2, and enabling multi-step ahead S_2 predictions with errors below 20.8% during closed-loop operation.

Although the $AM2HN_{obs}$ model was proven locally structurally observable, practical observability limitations due to the collinearity of states and parameters, confounding effects, and disparate time scales significantly affect EKF performance. Before closed-loop operations, practical observability and confounding analyses were therefore used to guide a principled tuning of the EKF, interpreted as an observability-informed shaping of $\mathbf{Q}$ rather than an *ad hoc* procedure.

Linearization of the model around the EKF operating trajectory and analysis of the associated observability Gramian $\mathbf{W_O}$ confirmed full rank but revealed significant ill-conditioning (condition number of $\approx 10^9$–10^{13}) and notable state coupling. In particular, methanogenic states (X_2, S_2) and ξ are the most observable due to their direct influence on the outputs (first-order impact looking at the output Jacobian), but exhibit significant mutual collinearity, while hydrolytic ($\mathbf{X_h}$) and acidogenic (X_1, S_1) states remain poorly observable. Additional confounding patterns (e.g., S_1–S_2, X_1–X_2) were found to be trajectory-dependent, highlighting a non-uniform and state-dependent observability structure (see Section III.D of the SM).

Accordingly, the EKF tuning prioritized correction along the most informative directions by assigning higher $\mathbf{Q}$ values to a subset of representative, well-observable states (S_2 and ξ in this case, see values in Table 1), while limiting process-noise inflation for strongly coupled or weakly observable states to avoid redundant correction channels and estimation drift. In contrast, directly measured states (e.g., $x_{M,gb}$) were assigned low $\mathbf{Q}$, as their estimation is primarily driven by measurements rather than model-based correction. This strategy effectively introduced an identifiability prior, whereby selected states absorb model mismatch while others remain more tightly constrained by the model (Schneider & Georgakis, 2013).

6. Conclusion and future work

This study presented the design and experimental validation of an output-feedback tube-based NMPC for the AcoD of agro-industrial feedstocks, built on an adapted and observable version of the AM2HN model and tested on a bench-scale reactor fed with a diet representative of full-

scale operation. An EKF, relying solely on *online* biogas flow rate and composition measurements, was jointly validated as the state observer underpinning the NMPC. Beyond satisfactory measurement filtering and open-loop model correction, the EKF successfully inferred TVFA, a key stability indicator, from the relative CH_4/CO_2 abundance in the biogas, as confirmed against *offline* measurements.

Both NMPC and selector-PI controllers tracked the biomethane flow rate reference defined by the *offline* agri-AcoDM optimization, safely increasing biomethane production by approximately 17–22% over the baseline. The tube-based NMPC was intentionally tuned with a robustness-oriented philosophy, incorporating explicit tightening of stability-related constraints, which favored safety and stability over aggressive biomethane production tracking. Since the selector-PI does not explicitly enforce state constraints, the comparison between the two strategies is inherently asymmetric, whereas, overall, the study highlights the intrinsic trade-off between robustness and economic performance in safety-critical AcoD control.

Future work will address: (i) extension of the EKF to a multi-rate setting incorporating delayed *offline* measurements (Elsheikh et al., 2021; Gudi et al., 1995); (ii) comparison with uncertainty-aware observers (e.g. H_∞ UKF Raeyatdoost et al., 2023); (iii) adaptive NMPC bounds and/or setpoints for a better robustness/tracking balance; and (iv) an *economic* NMPC formulation penalizing costly input feedstocks. The ultimate goal is a MIMO extension applicable to full-scale plants with automatic feeding of TS-rich feedstocks.

To the best of the authors' knowledge, this work provides the first experimental validation of a tube-based NMPC for agro-industrial AcoD, bridging robust control theory with practical bioprocess implementation. By enabling operation closer to user-defined safety limits, the proposed framework lays the foundation for improved techno-economic performance at industrial scale.

Glossary

The **bold** formatting refers to vectors in the variables' space, whereas the time dependency is implicit: when relevant, time indexing is explicitly reported as subscript.

$\odot$	Hadamard (element-wise) product
$a^{(b)}$	b^{th} entry of vector a
a_b, $a\|_b$	a evaluated at b
a_{lb}, a_{ub}	Lower, upper bounds of a
α, $\mu_{max,1}$, $\mu_{max,2}$, $K_{S,1}$, $K_{S,2}$, $K_{I,2}$, k_La	Process parameters of the AM2HN model
$\bar{a}$	Arithmetic mean a
$\hat{a}$	Estimation of a
$\tilde{a}$	Real measurement of a
AD, AcoD	Anaerobic Digestion, co-digestion
BMP	Biochemical Methane Potential
BMP_∞	Ultimate BMP
$\mathbf{BD_{VS_p}}$	Biodegradability of the $\mathbf{VS_p}$ ($\in \mathbb{R}^m$)
C	Dissolved inorganic carbon
C, N, P	Carbon, Nitrogen, Phosphorus
COD	Chemical Oxygen Demand
CSTR	Continuous-Stirred Tank Reactor
$\mathbf{COD_{X_h}/VS_{X_h}}$	COD over VS ratios of $\mathbf{X_h}$
D, HRT, OLR	Dilution rate, Hydraulic Retention Time, Organic Loading Rate
$\mathbf{d}$	Known disturbances, i.e. non-controllable input flow rates
Δt	Model integration time step
ΔT	Time distance from an (asynchronous) NMPC run to the previous one
du	Corrective control action of the selector-PI controller with respect to the equilibrium point of system's linearization, i.e. initial equilibrium
$\epsilon_{\tilde{y}}$	Relative sensors' errors ($\in \mathbb{R}^q$)
ϵ_{lb},ϵ_{ub}	Slack variables ($\in \mathbb{R}^n$)
IA, PA, TAC	Intermediate, Partial and Total Alkalinity
$\mathbf{f}$, $\mathbf{g}$	Vectors of nonlinear system's dynamics
FIM	Fisher Information Matrix
FOS/TAC	Ratio of organic acids (FOS) to Total Alkalinity (TAC)
gb	Subscript for quantities computed downstream of the gasbag
H_c	Control horizon
H_p	Prediction horizon
$k_{m,ac}$	Maximum methanogens' acetate uptake rate; $\boldsymbol{\theta_P}$ of the agri-AcoDM model
$k_{P,1}$, $k_{P,2}$, $T_{I,1}$, $T_{I,2}$	Tuning parameters of the selector-PI (1: q_M contr.; 2: $x_{C,gb}/x_{M,gb}$ contr.)
$\mathbf{k_h}$	Hydrolysis constants of $\mathbf{X_h}$ ($\in \mathbb{R}^m$)
lb, ub	Subscripts for lower/upper bounds
LHS	Latin Hypercube Sampling
m	Number of co-feedstocks in the input diet mixture
MIMO	Multiple-Input Multiple-Output
$MARE_{\%}$, r^2	Percentage Mean Absolute Relative Error, Pearson's coefficient of determination
MPC, NMPC	Model Predictive Control, Nonlinear MPC
μ_2	Methanogens' growth rate
n, q	Dimension of the $AM2HN_{obs}$ model states and *online* measurable outputs' vectors

N	Total Ammonia Nitrogen (TAN)
$\mathbf{N}_{\mathbf{X_h}}$	Nitrogen concentration in $\mathbf{X_h}$ ($\in \mathbb{R}^m$)
$N_{\tilde{y}}$	Number of data points in time for the $\tilde{y}$ measurable output
N_x	Nitrogen concentration in the microbial biomass (constant of the AM2HN model)
ODE, DAE	Ordinary Differential Equation, Differential Algebraic Equation
$\mathcal{O}$, $\mathbf{W}_{\mathcal{O}}$	Observability matrix, Obs. Gramian
$\mathbf{P}$	Error covariance matrix
P_{tot}	Total pressure of the reactor's headspace
q_C, q_M, q_{TOT}	Carbon dioxide, methane and total biogas flow rates
$\mathbf{Q}$, $\mathbf{R}$	Process and measurement noise covariance matrices
ref	Subscript for reference trajectories/controller setpoints
S_1, S_2	Soluble biodegradable COD and TVFA concentrations
SIMO	Single-Input Multiple-Output
SISO	Single-Input Single-Output
SM	Supplementary Material
t, k	Subscripts for time instances and control steps
T	Reactor's operating temperature
TVFA	Total Volatile Fatty Acids
TS, VS	Total and Volatile Solids
T_c	Control interval
$\mathbf{u}$	System's controllable inputs
V	Reactor's working volume
$\mathbf{VS_p}$	Particulate fraction of the VS ($\in \mathbb{R}^m$)
w_x, w_u, $w_{y_{H_p}}$	Weight of $\mathbf{z}^*$, $\boldsymbol{\nu}^*$ and terminal cost in NMPC *ancillary* problem's cost function
$w_{\epsilon_{lb}}$, $w_{\epsilon_{ub}}$	Weight of $\boldsymbol{\epsilon_{lb}}$,$\boldsymbol{\epsilon_{ub}}$ in NMPC *nominal* problem's cost function
$\mathbf{W_y}$	Setpoint weight matrix in the NMPC cost function
$\mathbf{x}$, $\mathbf{y}$	System states and outputs
$x_{M,gb}$, $x_{C,gb}$	CH_4 and CO_2 fractions in biogas after gasbag
$x_{C,gb}/x_{M,gb}$	Ratio between CO_2 and CH_4 biogas fractions
$(x_{C,gb}/x_{M,gb})_{ub,high}$, $(x_{C,gb}/x_{M,gb})_{ub,low}$	Hysteresis thresholds of the $x_{C,gb}/x_{M,gb}$ safety upper bound
X_1, X_2	Acidogens' and methanogens' biomass concentrations
$\mathbf{X_h}$	Biodegradable fraction of $\mathbf{VS_p}$ ($\in \mathbb{R}^m$)
ξ	Difference between Z and C
Z	Total Alkalinity (TAC)
$\mathbf{z}$, $\boldsymbol{\nu}$	Undisturbed/*nominal* system's state variables and inputs
$\mathbf{z}^*$, $\boldsymbol{\nu}^*$	States, inputs' solutions to the *nominal* NMPC optimization problem
$\mathbb{X}$, $\mathbb{Z}$	Feasible state sets of the *ancillary* and *nominal* NMPC problems
$\boldsymbol{\theta_{in,i}}$	Characterization of the i^{th} co-feedstock (as model's states)
$\boldsymbol{\theta_{kin}}$	Most relevant uncertain kinetic parameters of the AM2HN_{obs} model
$\boldsymbol{\theta_P}$	Uncertain process parameters
$\boldsymbol{\theta_{PSS}}$	$\boldsymbol{\theta_P}$ selected by the Parameter Subset Selection (PSS) algorithm
$\boldsymbol{\sigma_{\tilde{y}}}$	Measurements' standard deviations ($\in \mathbb{R}^q$)

CRediT authorship contribution statement

D. Carecci: Writing – original draft, Visualization, Software, Methodology, Investigation, Conceptualization; **L. Dewasme:** Writing – review & editing, Validation, Supervision, Methodology; **E. Ficara:** Writing – review & editing, Validation, Supervision, Conceptualization; **A. Vande Wouwer:** Writing – review & editing, Validation, Supervision, Methodology; **G. Ferretti:** Writing – review & editing, Validation, Supervision; **S. García-Gen:** Writing – review & editing, Validation, Supervision, Methodology.

Declaration of competing interest

The authors declare that they have no known competing financial interests or personal relationships that could have appeared to influence the work reported in this paper.

Acknowledgment

This work was supported by A2A S.p.A., the European Union and the Italian Ministry of University and Research (National Recovery and Resilience Plan, Mission 4, Component2, Investment 1.4 "National Research Center for Agricultural Technologies", Agritech CUP HUB - B63D21015240004). A special acknowledgment to Stefania Patronelli (R&D Project Manager, A2A S.p.A.) for her support.

Supplementary material

Supplementary material associated with this article can be found in the online version at 10.1016/j.conengprac.2026.107052.

References

Abbasi, T., Tauseef, S. M., & Abbasi, S. A. (2012). Anaerobic digestion for global warming control and energy generation-an overview. *Renewable and Sustainable Energy Reviews*, *16*(5), 3228–3242. https://doi.org/10.1016/j.rser.2012.02.046

Ahmed, W., & Rodríguez, J. (2020). A model predictive optimal control system for the practical automatic start-up of anaerobic digesters. *Water Research*, *174*, 115599. https://doi.org/10.1016/j.watres.2020.115599

Ahring, B., Sandberg, M., & Angelidaki, I. (1995). Volatile fatty acids as indicators of process imbalance in anaerobic digestors. *Applied Microbiology and Biotechnology*, *43*(3), 559–565. https://doi.org/10.1007/BF00218466

Alavi-Borazjani, S. A., Capela, I., & Tarelho, L. A. C. (2020). Over-acidification control strategies for enhanced biogas production from anaerobic digestion: A review. *Biomass and Bioenergy*, *143*, 105833. https://doi.org/10.1016/j.biombioe.2020.105833

APHA, AWWA, & WEF (2012). Standard methods for the examination of water and wastewater. (22nd ed.). Washington, DC: American Public Health Association.

Arzate, J. A., Kirstein, M., Ertem, F. C., Kielhorn, E., Ramirez M., H., Neubauer, P., Cruz-Bournazou, M. N., & Junne, S. (2017). Anaerobic digestion model (AM2) for the description of biogas processes at dynamic feedstock loading rates. *Chemie Ingenieur Technik*, *89*(5), 686–695. https://doi.org/10.1002/cite.201600176

Attar, S., & Haugen, F. (2018). Comparison of different state estimator algorithms applied to a simulated anaerobic digestion reactor. In *Proceedings of the 59th conference on simulation and modelling (SIMS 59)* (pp. 118–125). https://doi.org/10.3384/ecp18153118

Barahmand, Z., & Samarakoon, G. (2023). Anaerobic digestion process modeling under uncertainty: A narrative review. *International Journal of Energy Production and Management*, *8*, 41–54. https://doi.org/10.18280/ijepm.080106

Batstone, D. J., Keller, J., Angelidaki, I., Kalyuzhnyi, S. V., Pavlostathis, S. G., Rozzi, A., Sanders, W., Siegrist, H. a., & Vavilin, V. A. (2002). The IWA anaerobic digestion model no 1 (ADM1). *Water Science and Technology*, *45*(10), 65–73.

Bernard, O., Polit, M., Hadj-Sadok, Z., Pengov, M., Dochain, D., Estaben, M., & Labat, P. (2001). Advanced monitoring and control of anaerobic wastewater treatment plants: Software sensors and controllers for an anaerobic digester. *Water Science and Technology*, *43*(7), 175–182.

Bogaerts, P., & Wouwer, A. V. (2003). Software sensors for bioprocesses. *ISA Transactions*, *42*(4), 547–558.

Bornhöft, A., Hanke-Rauschenbach, R., & Sundmacher, K. (2013). Steady-state analysis of the anaerobic digestion model no. 1 (ADM1). *Nonlinear Dynamics*, *73*. https://doi.org/10.1007/s11071-013-0807-x

Brun, R., Reichert, P., & Künsch, H. R. (2001). Practical identifiability analysis of large environmental simulation models. *Water Resources Research*, *37*(4), 1015–1030. https://doi.org/10.1029/2000WR900350

Bułkowska, K., Białobrzewski, I., Klimiuk, E., & Pokoj, T. (2018). Kinetic parameters of volatile fatty acids uptake in the ADM1 as key factors for modeling co-digestion of silages with pig manure, thin stillage and glycerine phase. *Renewable Energy*, *126*, 163–176.

Carecci, D., Catenacci, A., Ficara, E., Ferretti, G., & Leva, A. (2024a). Modelling, optimisation and control of full-scale co-digestion biomethane plants. In *2024 IEEE 63rd conference on decision and control (CDC)* (pp. 106–112). https://doi.org/10.1109/CDC56724.2024.10886344

Carecci, D., Catenacci, A., Rossi, S., Casagli, F., Ferretti, G., Leva, A., & Ficara, E. (2024b). A plant-wide modelling framework to describe microalgae growth on liquid digestate in agro-zootechnical biomethane plants. *Chemical Engineering Journal*, *485*, 149981. https://doi.org/10.1016/j.cej.2024.149981

Carecci, D., Dewasme, L., La Bella, A., Ferretti, G., & Wouwer, A. V. (2025a). Tube-based robust nonlinear model predictive control of anaerobic co-digestion. In *2025 IEEE 64th conference on decision and control (CDC)* (pp. 6466–6473). https://doi.org/10.1109/CDC57313.2025.11312886

Carecci, D., Quarta, G., Catenacci, A., Ferretti, G., & Ficara, E. (2025b). Modelling of agro-zootechnical anaerobic co-digestion for full-scale applications. In *Systems and control transactions* (pp. 2310–2315). PSE Press (*vol. 4*). https://doi.org/10.69997/sct.193145

Dan, S. (2006). Optimal state estimation: Kalman, H-infinity, and nonlinear approaches. John Wiley & Sons, Ltd. https://doi.org/10.1002/0470045345.ch5

Dewasme, L., Mäkinen, M., & Chotteau, V. (2024). Multivariable robust tube-based nonlinear model predictive control of mammalian cell cultures. *Computers & Chemical Engineering*, *183*, 108592.

Dewasme, L., Sbarciog, M., Rocha-Cózatl, E., Haugen, F., & Vande Wouwer, A. (2019). State and unknown input estimation of an anaerobic digestion reactor with experimental validation. *Control Engineering Practice*, *85*, 280–289.

Dochain, D., & Vanrolleghem, P. (2005). Dynamical modelling & Estimation in wastewater treatment processes. IWA Publishing. https://doi.org/10.2166/9781780403045

Díaz-Seoane, S., Rey Barreiro, X., & Villaverde, A. F. (2022). Strike-goldd 4.0: User-friendly, efficient analysis of structural identifiability and observability. *Bioinformatics*, *39*(1), btac748. https://doi.org/10.1093/bioinformatics/btac748

Elsheikh, M., Hille, R., Tatulea-Codrean, A., & Krämer, S. (2021). A comparative review of multi-rate moving horizon estimation schemes for bioprocess applications. *Computers & Chemical Engineering*, *146*, 107219. https://doi.org/10.1016/j.compchemeng.2020.107219

European Biogas Association (2024). EBA statistical report 2024. Technical Report European Biogas Association. https://www.europeanbiogas.eu/eba-statistical-report-2024/.

Gudi, R. D., Shah, S. L., & Gray, M. R. (1995). Adaptive multirate state and parameter estimation strategies with application to a bioreactor. *AIChE Journal*, *41*(11), 2451–2464. https://doi.org/10.1002/aic.690411111

Hassam, S., Ficara, E., Leva, A., & Harmand, J., et al. (2015). A generic and systematic procedure to derive a simplified model from the anaerobic digestion model no. 1 (ADM1). *Biochemical Engineering Journal*, *99*, 193–203. https://doi.org/10.1016/j.bej.2015.03.007

Hellmann, S., Frontzek, J., Zarate, D. M., Wilms, T., Koch, K., Knorn, S., Streif, S., & Weinrich, S. (2026). Multi-stage model predictive control of agricultural anaerobic digestion plant with uncertain substrate characterization. *Bioresource Technology*, *441*, 133568. https://doi.org/10.1016/j.biortech.2025.133568

Hellmann, S., Hempel, A.-J., Streif, S., & Weinrich, S. (2023). Observability and identifiability analyses of process models for agricultural anaerobic digestion plants. In *2023 24th International conference on process control (PC)* (pp. 84–89). https://doi.org/10.1109/PC58330.2023.10217587

Holliger, C., Alves, M., Andrade, D., Angelidaki, I., Astals, S., Baier, U., Bougrier, C., Buffière, P., Carballa, M., de Wilde, V., Ebertseder, F., Fernández, B., Ficara, E., Fotidis, I., Frigon, J.-C., de Laclos, H. F., Ghasimi, D. S. M., Hack, G., Hartel, M., Heerenklage, J., Horvath, I. S., Jenicek, P., Koch, K., Krautwald, J., Lizasoain, J., Liu, J., Mosberger, L., Nistor, M., Oechsner, H., Oliveira, J. V., Paterson, M., Pauss, A., Pommier, S., Porqueddu, I., Raposo, F., Ribeiro, T., Rüsch Pfund, F., Strömberg, S., Torrijos, M., van Eekert, M., van Lier, J., Wedwitschka, H., & Wierinck, I. (2016). Towards a standardization of biomethane potential tests. *Water Science and Technology*, *74*(11), 2515–2522. https://doi.org/10.2166/wst.2016.336

Ibarra-Esparza, J., Ibarra-Esparza, F. E., González-López, M. E., Garcia-Gonzalez, A., & Gradilla-Hernández, M. S. (2025). Instrumentation and continuous monitoring for the anaerobic digestion process: A systematic review. *IEEE Access*, (pp. 1–1). https://doi.org/10.1109/ACCESS.2025.3623647

Jimenez, J., Latrille, E., Harmand, J., Robles, A., Ferrer, J., Gaida, D., Wolf, C., Mairet, F., Bernard, O., Alcaraz-Gonzalez, V. et al. (2015). Instrumentation and control of anaerobic digestion processes: A review and some research challenges. *Reviews in Environmental Science and Bio/Technology*, *14*, 615–648.

Kazemi, P., Giralt, J., Bengoa, C., & Steyer, J.-P. (2020). Data-driven fault detection methods for detecting small-magnitude faults in anaerobic digestion process. *Water Science and Technology*, *81*(8), 1740–1748. https://doi.org/10.2166/wst.2020.026

Kegl, T., Torres Jiménez, E., Kegl, B., Kovač Kralj, A., & Kegl, M. (2025). Modeling and optimization of anaerobic digestion technology: Current status and future outlook. *Progress in Energy and Combustion Science*, *106*, 101199. https://doi.org/10.1016/j.pecs.2024.101199

Mauky, E., Weinrich, S., Nägele, H.-J., Jacobi, H. F., Liebetrau, J., & Nelles, M. (2016). Model predictive control for demand-driven biogas production in full scale. *Chemical Engineering & Technology*, *39*(4), 652–664.

Mayne, D. Q., Kerrigan, E. C., van Wyk, E. J., & Falugi, P. (2011). Tube-based robust nonlinear model predictive control. *International Journal of Robust and Nonlinear Control*, *21*(11), 1341–1353. https://doi.org/10.1002/rnc.1758

Nimmegeers, P., Lauwers, J., Telen, D., Logist, F., & Impe, J. V. (2017). Identifiability of large-scale non-linear dynamic network models applied to the ADM1-case study. *Mathematical Biosciences*, *288*, 21–34. https://doi.org/10.1016/j.mbs.2017.02.008

Piceno-Díaz, E. R., Ricardez-Sandoval, L. A., Gutierrez-Limon, M. A., Méndez-Acosta, H. O., & Puebla, H. (2020). Robust nonlinear model predictive control for two-stage anaerobic digesters. *Industrial & Engineering Chemistry Research*, *59*(52), 22559–22572. https://doi.org/10.1021/acs.iecr.0c03809

Raeyatdoost, N., Bongards, M., Bäck, T., & Wolf, C. (2023). Robust state estimation of the anaerobic digestion process for municipal organic waste using an unscented Kalman filter. *Journal of Process Control*, *121*, 50–59. https://doi.org/10.1016/j.jprocont.2022.11.013

Schneider, R., & Georgakis, C. (2013). How to not make the extended Kalman filter fail. *Industrial & Engineering Chemistry Research*, *52*(9), 3354–3362. https://doi.org/10.1021/ie300415d

Vavilin, V. A., & Lokshina, L. Y. (1996). Modeling of volatile fatty acids degradation kinetics and evaluation of microorganism activity. *Bioresource Technology*, *57*(1), 69–80.

Weinrich, S., & Nelles, M. (2021). Basics of anaerobic digestion - biochemical conversion and process modelling. DBFZ Deutsches Biomasse Forschungs Zentrumgemeinnützige GmbH, Leipzig, Germany.

Zhou, H., Ying, Z., Cao, Z., Liu, Z., Zhang, Z., & Liu, W. (2020). Feeding control of anaerobic co-digestion of waste activated sludge and corn silage performed by rule-based pid control with ADM1. *Waste Management*, *103*, 22–31.